Journal of Bioscience and Bioengineering
VOL. 128 No. 1, 110–116, 2019

ELSEVIER

www.elsevier.com/locate/jbiosc

Combined apoptotic effects of peptide and miRNA in a peptide/miRNA nanocomplex

Hyungjin Kim,[1] Mizuki Kitamatsu,[2] and Takashi Ohtsuki[1,*]

Department of Interdisciplinary Science and Engineering in Health Systems, Okayama University, 3-1-1 Tsushimanaka, Okayama 700-8530, Japan[1] and Department of Applied Chemistry, Kindai University, 3-4-1 Kowakae, Higashi-Osaka, Osaka 577-8502, Japan[2]

Received 7 September 2018; accepted 11 January 2019
Available online 2 February 2019

The present study investigated combined biological effects of peptide and miRNA in a peptide/miRNA nanocomplex. We utilized TatBim peptide as a cell-penetrating peptide-based RNA carrier with apoptotic activity. miRNA with apoptotic activity (miR-34a) was used for complex formation to investigate the additional effects of the combination with TatBim peptide. TatBim peptide and the miRNA formed nanocomplexes (approximately 250 nm in diameter), and these complexes were efficiently internalized by cells. Despite its efficient cell internalization, apoptotic activity of the nanocomplex decreased with increasing RNA content. However, photosensitizer-attachment to TatBim and photoirradiation significantly improved the apoptotic activity of the nanocomplex by facilitating dispersion of the peptide and RNA in the cytoplasm. Combined apoptotic activity of both TatBim peptide and miR-34a in the nanocomplex was demonstrated by substituting TatBim with Lipofectamine and by substituting miR-34a with scrambled siRNA.

[**Key words:** Cell-penetrating peptide; Nanocomplex; TatBim; miRNA; Apoptosis; Photosensitizer]

MicroRNAs (miRNAs) are 20–25 nucleotide-long, noncoding RNAs, which post-transcriptionally downregulate the expression of multiple genes, by base-pairing with the 3′ untranslated region of messenger RNAs (mRNAs). Discovery of their critical roles in various biological processes, including differentiation (1,2), development (3,4), metabolism (5,6), proliferation, cell death, and tumorigenesis (7) have inspired the exploration of miRNAs as therapeutic agents (8,9). However, RNA therapeutic success has been limited by poor cellular uptake, because of their high molecular weight and strong negative charge. These problems, along with degradation of free RNA by endonucleases in serum, have necessitated the designing of delivery systems that protect RNA and promote its uptake by cells.

Cell penetrating peptides (CPPs), which are 8–30 amino acids long and comprise cationic or amphipathic sequences, can be promising RNA delivery vectors. They can efficiently deliver a covalently or non-covalently (electrostatically) bound nucleic acid into cells with low accompanying cytotoxicity (10–13). CPP-mediated RNA delivery is usually achieved by non-covalent complex formation between anionic RNA and cationic CPP. These complexes are easy to prepare and do not disrupt the formation of RNA-induced silencing complex (14). Despite the enhanced cellular uptake of RNA by non-covalent complex formation with molar excess of cationic CPP, the functionality of the delivered RNA is often limited by endosomal entrapment, resulting in the loss of its pharmacological activity. For this reason, dual functional CPPs that complex with RNA and disrupt endosomal compartments have been designed (15–19).

Despite the sophisticated design of CPP carriers for enhanced RNA delivery, their role has been restricted to being mere excipients for RNA vector and/or endosomal escape. In other words, CPP carriers did not exert any biological effects such as differentiation, proliferation, and apoptotic cell death. As a CPP-based RNA carrier with apoptotic activity, we here utilized TatBim peptide (20,21), which is a fusion of TAT CPP derived from the HIV-1 TAT protein and Bim peptide derived from Bim apoptosis-inducing protein. Overexpression of Bim in cancer cells results in tumor death by mediating the release of cytochrome C from mitochondria. In this study, an miRNA that induces apoptosis or cell cycle arrest (miR-34a) (22–24) was used to investigated the additional apoptotic effect combined with TatBim peptide. By using TatBim peptide and miR-34a, the structure and in vitro function of peptide/miRNA complexes were investigated.

MATERIALS AND METHODS

Materials Tetramethylrhodamine maleimide (TMR) and Alexa Fluor 546C_5 maleimide (Alexa546) were from Molecular Probes, Inc. (Eugene, OR, USA). NucView488 was from Biotium, Inc. (Fremont, CA, USA). Cell Counting Kit-8 was obtained from Dojindo Laboratories (Kumamoto, Japan). Fetal bovine serum (FBS) was obtained from Japan Bioserum (Hiroshima, Japan). Dulbecco's phosphate buffered saline (PBS) and trypsin–EDTA (0.05% trypsin, 0.53 mM EDTA-4Na) were obtained from Invitrogen (Carlsbad, CA, USA). RPMI1640 media were purchased from Nacalai Tesque (Kyoto, Japan). Cell culture dishes were from BD Bioscience (San Jose, CA, USA). TatBim peptide (Fig. 1A) was prepared by the conventional Fmoc-based solid-phase peptide synthesis method.

* Corresponding author. Tel.: +81 251 8218; fax: +81 251 8219.
E-mail address: ohtsuk@okayama-u.ac.jp (T. Ohtsuki).

1389-1723/$ – see front matter
https://doi.org/10.1016/j.jbiosc.2019.01.003

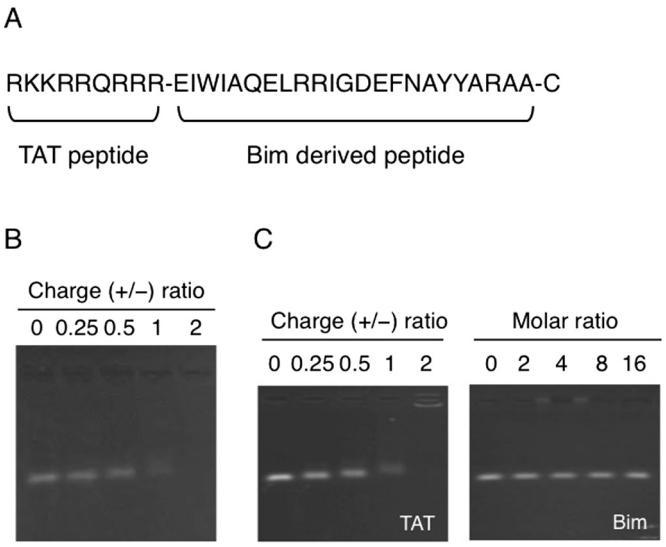

FIG. 1. TatBim peptide interacted with miRNA via cation-rich TAT segment. (A) Amino acids sequence of TatBim peptide. (B) TatBim/miRNA complexes (miRNA 5 pmol/lane) prepared at indicated charge ratios (±) were analyzed by agarose gel (0.8% wt/vol) mobility shift assay. (C) Two segments in TatBim peptide, TAT and Bim, were separately synthesized to identify the domain that interacts with miRNA. Because of the total anionic charge of Bim, Bim/miRNA complexes were formed using molar ratios corresponding to charge ratios of TAT/miRNA complexes.

Preparation of miR-34a and scrambled siRNA miR-34a mimic was designed as an RNA duplex with miR-34a mimic-sense (5′-UGGCAGUGUCUUAGCUGGUUGUU-3′) and miR-34a mimic-antisense (5′-CAACCAGCUAAGACACUGCCACU-3′). miR-34a mimic-antisense labeled with 3′-fluorescein (FAM) was also prepared for investigation of cell internalization. Hereafter, this sequence is referred to as miR-34a. The small interference scrambled RNA duplex (siSc) with siRNA scrambled-sense (5′-AUCUCGCUUGGGCGAGAGUAAGTT -3′) and siRNA scrambled-antisense (5′-CUUACUCUCGCCCAAGCGAGAUTT -3′) was used as a negative control for miR-34a. All RNA oligos were provided via a custom RNA synthesis service from Japan Bio Services Co., Ltd. (Saitama, Japan) with MS and HPLC data ensuring their molecular mass and purity.

Agarose gel mobility shift assay To prepare peptide/miRNA complexes, TatBim peptide and miRNA (100 ng) were incubated for 15 min at 25°C in ultrapure water with varying concentrations of TatBim solutions, corresponding to charge ratio (±) ranging from 0 to 20. These mixtures were subjected to agarose gel (0.8% wt/vol) electrophoresis in 50 mM HEPES buffer (pH 7.6), to analyze TatBim/miRNA (100 ng miRNA/lane) complex formation. Agarose gel was pre-stained with ethidium bromide to visualize the miRNA in the complex.

Dynamic light scattering and zeta-potential analysis TatBim peptide (1 nmol) was incubated in ultrapure water at 25°C for 15 min with different amounts of miR-34a, corresponding to charge ratios between 2 and 20. The diameter distribution of the TatBim/miRNA complexes was determined using a Zetasizer Nano ZS (Malvern, Worcestershire, UK) with a He–Ne laser at a wavelength of 633 nm (scattering angle of 173°). Zeta potential of the TatBim/miRNA complexes was also measured using a Zetasizer Nano ZS.

Cell culture HeLa cells obtained from ATCC (Manassas, VA, USA) were maintained/cultured in RPMI 1640 medium supplemented with 10% FBS. All cell culture media contained 100 U/mL penicillin and 100 μg/mL streptomycin. For some experiments, cells were incubated in serum-free media. Cells were incubated at 37°C in a humidified atmosphere of 5% CO_2 and 95% air. Cells were passaged every 3–4 days.

Cellular internalization of TatBim/FAM-shRNA nanocomplex TatBim was reacted with TMR at a peptide:TMR molar ratio of 10:1, in DMSO at 37°C for 2 h. The reaction mixture was then subjected to HPLC to eliminate unreacted TMR. The cells were seeded at 2.0×10^4 cells/well in 96-well plate and cultured for a day. The cells were then treated with TMR-labeled TatBim/FAM-shRNA complexes including 10 μM peptide for 2 h at 37°C in serum free medium. After 2 h, 0.04% trypan blue in PBS (wt/vol) was added for 1 min at 25°C, to quench the fluorescence from complexes bound to cell surface. The cells were washed twice with complete medium supplemented with 10% FBS. Fluorescence images were acquired using an Olympus IX51 fluorescent microscope (Olympus, Tokyo, Japan).

Photoinduced dispersion of TatBim/FAM-shRNA complex Alexa Fluor 546C_5 maleimide (Alexa546), a photosensitizer, was conjugated to the thiol group of cysteine residue located in the C-terminus of the TatBim at a peptide:Alexa546 M ratio of 1:1 in DMF at 85°C for 1 h. The reaction mixture was then subjected to HPLC, to eliminate the unreacted Alexa546. TatBim bound Alexa546 to the extent of 30% (data not shown). The cells were then subjected to the same treatment as in the section entitled "cellular internalization of TatBim/FAM-shRNA nanocomplex". After the treatment, the cells were photoirradiated at 540 ± 10 nm at a fluence of 50 J/cm^2.

Apoptosis assay The cells (2×10^4 cells/well) were seeded in a 96-well plate. After a day, the cells were treated with TatBim/miR-34a complexes including 10 μM peptide for 2 h at 37°C in a serum-free medium. The medium was then changed to complete medium supplemented with 10% FBS and 1 μM NucView488, to detect caspase-3/7 activity. Green fluorescence images were captured by microscopy, after 30 min of NucView488 treatment.

Cell proliferation assay Cells were treated for 2 h with TatBim/miR-34a complexes (10 μM TatBim) or 6 h with Alexa546-attached complexes (2.5 and 5 μM TatBim). The cells treated with Alexa546-attached complexes were subjected to photoirradiation. At two days after the irradiation, cell proliferation was evaluated using a Cell Counting Kit-8 and a model 680 microplate reader (Bio-Rad, Hercules, CA, USA). Cell proliferation was normalized relative to that of untreated cells ($A_{450} - A_{620}$). Assays were performed in triplicate.

RESULTS

Ability of TatBim peptide to associate with miR-34a TatBim peptide (Net charge = +7) with a C-terminal $CONH_2$ was prepared to investigate their ability to interact with miR-34a (Net charge = −46; the number of phosphate) (Fig. 1A). Net charge of TatBim was determined by calculating the sum of amino acid charge at neutral pH. TatBim was over 90% pure, as demonstrated by HPLC analysis (Fig. S1). The RNA (5 pmol) was incubated for 15 min at 25°C with TatBim at indicated charge ratios (±), in ultrapure water. Mobility shift of miR-34a was assessed by agarose gel (0.8% wt/vol) electrophoresis at pH 7.4. As shown in Fig. 1B, the RNAs started interacting with all TatBim at a charge ratio of 0.25 and the association was complete at a charge ratio of 2, indicating that anionic charge of miRNA can be neutralized by TatBim via electrostatic interaction. TatBim/miRNA complexes prepared at a charge ratio ≥2 did not migrate into the agarose gel and no free miRNA was detected on the agarose gel, indicating the formation of high-molecular weight complexes.

To elucidate the interaction domain of TatBim with miRNA, TAT peptide (YGRKKRRQRRRC with net charge of +8) and Bim peptide (EIWIAQELRRIGDEFNAYYARAAC with net charge of −1) were also synthesized. Because of the anionic net charge of the Bim peptide, charge ratios of the Bim/miRNA complexes were converted to molar ratios (peptide/miRNA), which corresponded to charge ratios of TAT/miRNA complexes. The TAT-miRNA interaction was complete at the charge ratio of 2 (molar ratio of 16), but no miRNAs associated with Bim even at a molar ratio of 16 (Fig. 1C), suggesting that cation-rich TAT segment in TatBim contributed to complex formation.

Characterization of TatBim/miRNA complexes Table 1 summarizes the diameters and zeta-potentials of TatBim/miRNA complexes. These parameters were measured using complexes that included 1 μM peptide and miRNA at charge ratios between 2 and 20. Mean diameters of all samples ranged from 215 to 330 nm. Zeta-potentials of all complexes were approximately 20–30 mV, suggesting that the surface of the complex mainly

TABLE 1. Diameter and zeta-potential of TatBim/miR-34a complexes.

Charge ratio (±)[a]	Diameter/nm	PDI[b]	Zeta-potential/mV
2	215.8 ± 6.0	0.25 ± 0.01	27.9 ± 1.5
5	265.3 ± 12.0	0.05 ± 0.02	30.5 ± 1.9
10	291.2 ± 5.9	0.15 ± 0.04	30.0 ± 1.7
20	333.4 ± 35.9	0.17 ± 0.08	27.4 ± 2.1

[a] TatBim peptide (500 μM in water) was mixed with different amounts of the RNA to prepare complexes with different charge ratios. The resultant complexes were diluted 500-fold with water.

[b] PDI means polydispersity index. All results represent means ± S.D. (n = 3).

comprised TatBim molecules. There was no clear correlation between the charge ratio and the zeta-potential of the complexes.

Morphology of the TatBim/miRNA nanocomplex (charge ratio 10) was investigated by transmission electron microscopy (TEM) and scanning transmission electron microscopy (STEM). A few bean-like structures of 250–300 nm in diameter (Fig. 2A and B), which was consistent with the dynamic light scattering (DLS) data (Table 1), were observed. To confirm the chemical composition of the nanocomplex observed in STEM image, we performed atom mapping of the area depicted in Fig. 2B, using energy dispersive X-ray spectroscopy (EDS). Oxygen (Fig. 2C) and phosphorus atoms (Fig. 2D) in the nanocomplex in Fig. 2B were mapped. Oxygen present in both peptide and miRNA (Fig. 2C) and phosphorus present only in the miRNA (Fig. 2D) were clearly detected and distributed all over the nanocomplex, demonstrating that it was composed of peptide and miRNA.

Cellular internalization of TatBim/miRNA nanocomplexes To analyze the cellular internalization of nanocomplexes, HeLa cells were treated with fluorescently labeled TatBim/miRNA complexes. TatBim was labeled with TMR. miRNA labeled with 3'-fluorescein (FAM) in antisense strand was used for investigation of cellular internalization. The cells were treated with TatBim/miRNA complex including 10 μM peptide, in the absence of serum. TatBim was efficiently internalized by cells irrespective of charge ratio. There was no significant difference in the uptake quantities of the complex and peptide alone (Fig. 3), indicating that coexistence with the RNA did not hinder cellular internalization of the peptide. Positive surface charges (≥25 mV, Table 1) of TatBim/miRNA nanocomplexes presenting TAT peptide on the surface might potentiate the internalization of the complexes. miRNA was also efficiently internalized by the cell along with the bound peptide (Fig. 3). The amount of internalized miRNA increased gradually with decreasing charge ratio, because of its higher content in the complexes with lower charge ratio. The two components of the nanocomplex were mostly co-localized in the cells in punctuation state, suggesting that the nanocomplexes were internalized without breaking down for at least 2 h.

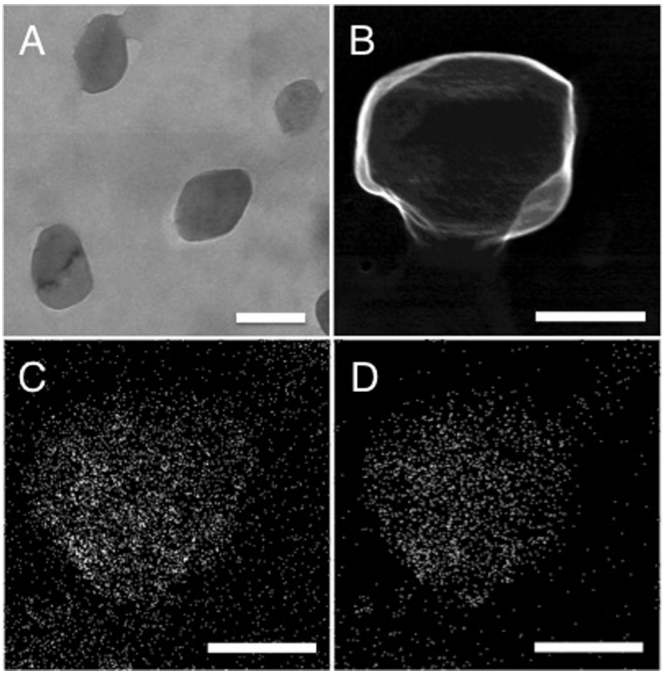

FIG. 2. TatBim formed approximately 250 nm-sized complexes with miR-34a. (A) Morphology of the complex prepared at charge ratio of 10 was measured by TEM. (B) Bright field image of the nanocomplex observed by STEM. (C, D) Distribution of (C) oxygen and (D) phosphorus atoms was observed by EDS mapping. Panels B–D depict the same area. Scale bar: 200 nm.

Apoptosis activity of TatBim/miR-34a nanocomplexe TatBim at 10 μM induces apoptosis (35–64%) in various cancer cell lines, including EL4 (T-cell lymphoma), Panc-02 (pancreatic cancer), and B16 (melanoma) (20). Apoptosis activity after the treatment was evaluated by detecting the activated caspase-3/7 using NucView488. Treatment with TatBim without miR-34a showed the most potent apoptotic activity (Fig. 4B), but decreased gradually with increasing content of miR-34a in the nanocomplex and almost disappeared at a charge ratio of 2, which included the largest amount of miR-34a (Fig. 4C–F). The degree of reduction was proportional to the increase in miRNA quantity. The RNA in the complex might be hindering the activity of the bound peptide as well as its own activity, without affecting the internalization of the peptide, as shown in Fig. 3. It is thought that electrostatic interaction between the multiple anionic charges of miRNA and cationic TAT moiety might inhibit the release of both TatBim and miRNA into the intracellular compartment (25–27). Consistent with the results of the apoptosis assay, cell proliferation was also inhibited strongly by treatment with TatBim alone and increased gradually with increasing content of miR-34a (Fig. 4G).

Cytoplasmic dispersion of photosensitizer-attached TatBim/RNA nanocomplexes and photoenhanced activity of the nanocomplex In an earlier study, we developed a TAT peptide fused RNA binding protein (TAT-RBP) as an RNA carrier and demonstrated that the photosensitizer-attached TAT-RBP/RNA complex was efficiently dispersed in the cytoplasm by photoirradiation (28–30). Irradiation of the photosensitizer-attached TAT-RBP/RNA complex can induce reactive oxygen species generation, which can lead to destabilization of the endosomal membrane and dispersion of the complex from the endosomes (31). Therefore, a photosensitizer, Alexa Fluor 546C_5 maleimide (Alexa546) was attached to the C-terminus of TatBim, to facilitate the dispersion of the peptide and RNA in the cytoplasm. TatBim bound to Alexa546 to the extent of 30%. The attachment of Alexa546 did not affect the association ability of TatBim with miR-34a (Fig. S2). Cells were treated with the complexes of Alexa546-attached TatBim (2.5 μM) and FAM-labeled miRNA to investigate the light-induced dispersion of the nanocomplex in the cytoplasm. Because of the lower peptide concentration compared to that shown in Fig. 2 (10 μM), the treatment period was prolonged by 6 h to increase the internalized amount of the nanocomplex. Before irradiation, TatBim and the miRNA were mainly observed in a punctuate distribution, indicating their localization in endocytic compartments. TatBim and miRNA co-localized well (Fig. 5), similar to TMR-labeled TatBim/miRNA complex (Fig. 3). After irradiation, diffuse and increment of Alexa546 signals in the cytoplasm were observed from the complex under charge ratio 10. Interestingly, cytosolic Alexa546 signals augmented with the decrease of charge ratio (Fig. 5). Increase in RNA content in the nanocomplex induced an increase in TatBim dispersion in the cytosol. Given that increasing the RNA content significantly affected the size of the nanocomplex but not its zeta-potential (Table 1), decreasing the size of the nanocomplexes with increase in RNA content may be the cause of the acceleration of photoinduced TatBim dispersion. The RNA was also efficiently dispersed after irradiation, especially in the complexes with high RNA content. The internalized amount of the RNA with the complex (charge ratio 2.5) was significantly higher than that in commercial lipofection reagent, Lipofectamine RNAiMAX (Life

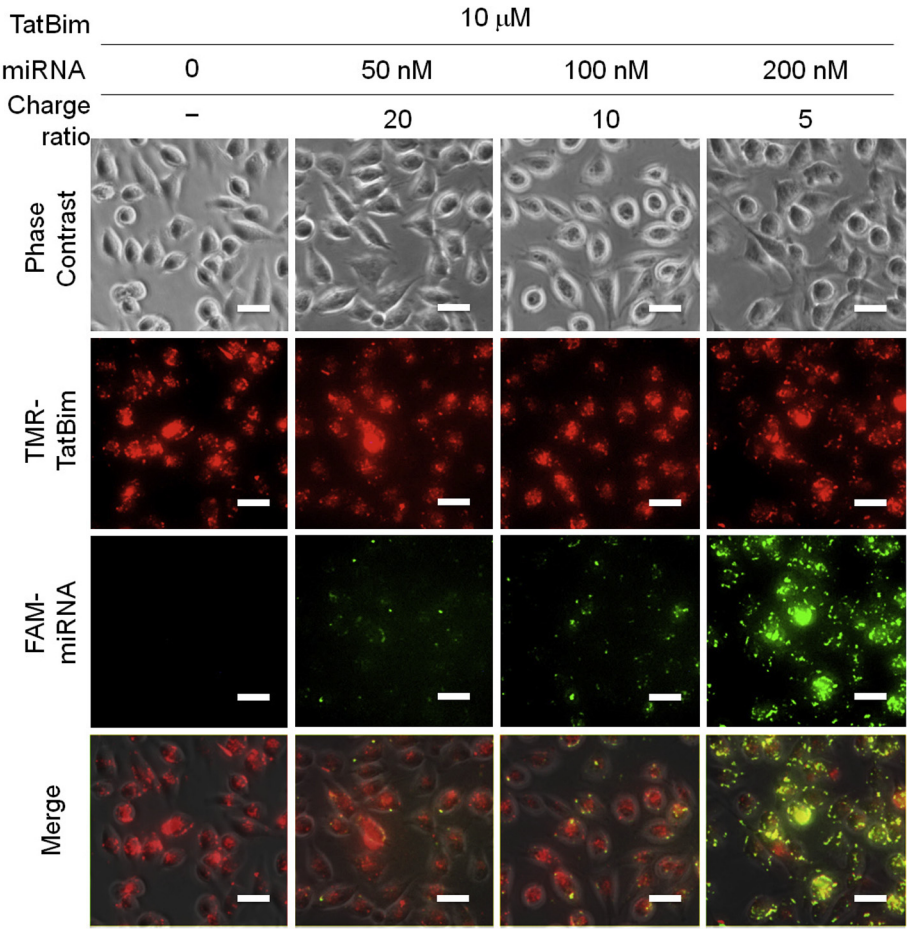

FIG. 3. TatBim/miRNA nanocomplexes were efficiently internalized by HeLa cells. TatBim was fluorescently labeled with tetramethylrhodamine (TMR) (see Materials and methods), and miRNA, targeting luciferase, was labeled with fluorescein (FAM). HeLa cells were treated with TatBim/miRNA complexes including 10 μM peptide for 2 h at 37°C in the absence of serum. Scale bar: 20 μm.

Technologies, Carlsbad, CA, USA) (Fig. S3). Increment of overall Alexa546 and FAM signals after dispersion might be explained by different pH environments between the endosome (mildly acidic pH) and cytoplasm (neutral pH) (31). In addition, concentration quenching in the endosomes might be canceled after cytosolic dispersion of the fluorophores.

Photo-dependent dissociation of the nanocomplex was investigated in vitro using agarose gel electrophoresis. Alexa546-

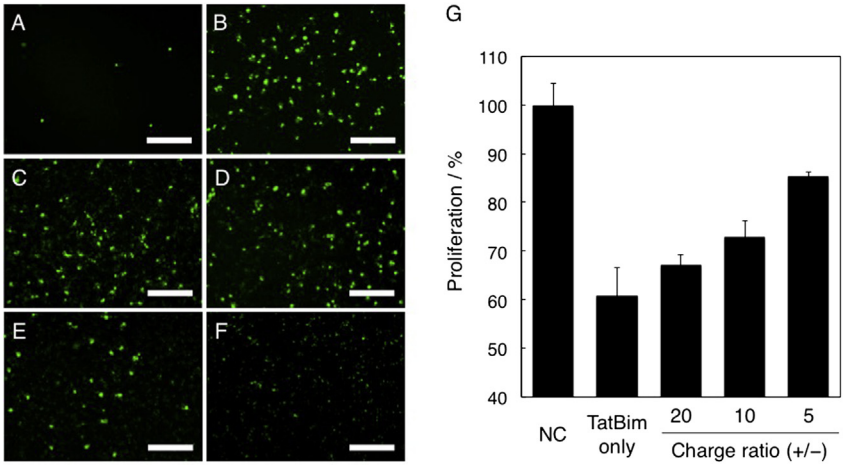

FIG. 4. Apoptotic activity of TatBim/miR-34a nanocomplex decreases with increasing quantities of RNA in the nanocomplex. HeLa cells were treated with the nanocomplex including 10 μM TatBim. (A–F) Apoptosis assay was performed after treatment, using NucView488, which evaluates the activity of caspase-3. (A) No treatment, (B) TatBim alone, and (C–F) the nanocomplexes prepared with charge ratios 20, 10, 5 and 2, in that order. (G) Proliferation assay was performed at 18 h after treatment with the nanocomplex ($n = 3$). NC means negative control using media only. Scale bar: 100 μm.

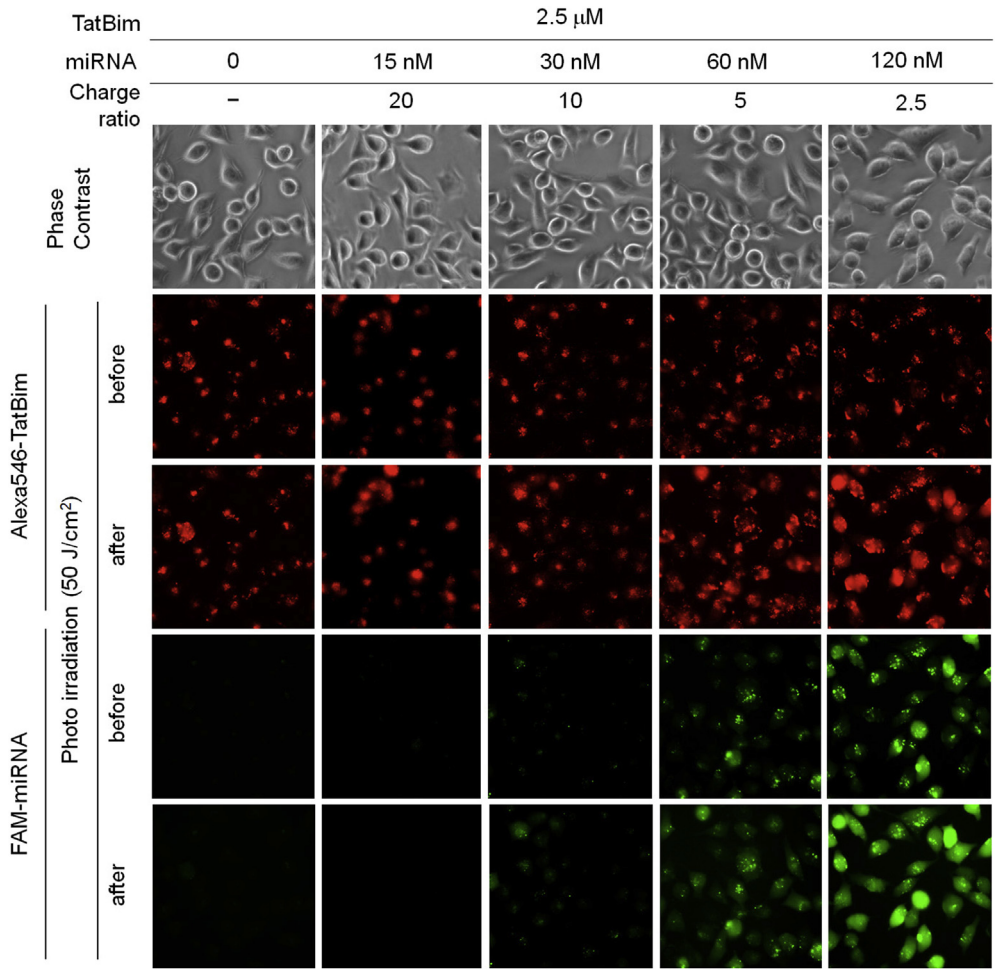

FIG. 5. Photosensitizer-attached nanocomplexes with low charge ratio efficiently dispersed in the cytoplasm after photoirradiation. HeLa cells were treated with Alexa546-attached TatBim/miRNA complexes including 2.5 μM peptide for 6 h at 37°C in the absence of serum. After the treatment, the cells were irradiated at 540 ± 10 nm at a fluence of 50 J/cm^2. Scale bar: 20 μm.

attached TatBim/miRNA nanocomplex with charge ratio 5 was irradiated and loaded onto an agarose gel. As shown in Fig. S4A, dissociated miRNA levels increased depending on the light energy density. Next, nanocomplexes with different charge ratios were irradiated to examine the charge ratio-dependent cytosolic dispersion of miRNA. Fig. S4B shows that the released miRNA levels increased with a decrease in the charge ratio, which is consistent with Fig. 5. The mechanism of this phenomenon is not clear for now and needs to be investigated further. However, it should be noted that lower charge ratio-dependent dissociation of the nanocomplex was observed in cells and in vitro despite entirely different environments (e.g., ionic strength, viscosity, pH) between them.

Next, we evaluated the proliferation of cells treated with Alexa546-attached nanocomplex, after photoirradiation. When the cells were treated with the samples including 5 μM of TatBim, their proliferation decreased to less than 47%, and no significant difference was observed among the nanocomplexes with different charge ratios (Fig. 6A). Compared with Fig. 4G, Fig. 6A clearly shows that the reduced apoptotic activity of nanocomplex related to the RNA content is rescued by the light-dependent breakdown of the nanocomplex and dispersion of the components. In case of the treatment with 2.5 μM TatBim, only the nanocomplex with a charge ratio of 2.5 could significantly inhibit cell proliferation (45%) (Fig. 6A). This photo-enhanced apoptotic activity and cell proliferation inhibiting ability of the nanocomplex (charge ratio 2.5, compared to Fig. S5) seems to be due to the cytoplasmic dispersion of the peptide and RNA (Fig. 5). Next, we investigated the contribution of the peptide and the RNA on this enhanced apoptotic activity. Substitution of miR-34a with scrambled siRNA (siSc, 48 mer) that is not involved in apoptosis increased the cell proliferation from 54% to 67% (Fig. 6B) indicating that internalization and dispersion of miR-34a partially contributed to the apoptotic activity of the nanocomplex. An increase from 54% to 73% with the substitution of TatBim to Lipofectamine RNAiMAX indicates that the contribution of TatBim to the apoptotic activity of the nanocomplex is greater than that by miR-34a.

DISCUSSION

TatBim was used here as the peptide with dual functions of RNA carrier and apoptotic inducer. There are relatively limited number of reports on the development of dual functional nucleic acid-carriers that have both a delivery function as well as a pharmacological activity to enhance the therapeutic outcome of gene and RNA interference therapies (32,33). Li et al. (32) reported a polycation that not only delivers plasmid DNA but also works as a CXCR4 antagonist to inhibit cancer cell invasion. However, the biological activity of polycations decreased with increasing content of DNA in a polycation/DNA complex. A similar tendency was also observed in CXCR4-targeted RNA condensing peptide (33). Similar to these previous reports, the apoptotic activity of TatBim peptide

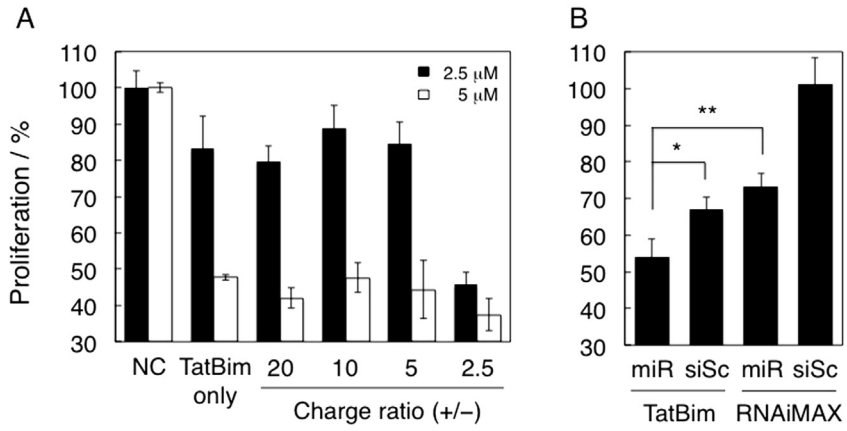

FIG. 6. Enhanced apoptotic activity of a nanocomplex compared to the single component (peptide or RNA). (A) HeLa cells were subjected to the same treatment as described in Fig. 5, with the indicated peptide concentration (closed bars, 2.5 μM; open bars, 5 μM). After the treatment, the cells were irradiated at 540 ± 10 nm at a fluence of 50 J/cm^2. (B) miR-34a in the nanocomplexes with a charge ratio of 2.5 was substituted with scrambled siRNA (siSc) that has no apoptotic activity and has comparable nucleotide length (48 mer), to evaluate the contribution of miR-34a to apoptotic activity. Lipofectamine RNAiMAX was used as a substitute for TatBim. The cells were irradiated at 50 J/cm^2. Proliferation assay was performed for two days after photoirradiation (n = 3). NC means negative control using media only. $^*p < 0.05$, $^{**}p < 0.01$.

decreased gradually with increasing RNA content in the nanocomplex. It should be noted that the TatBim has an intracellular activity, not an on-cell activity such as the CXCR4 antagonist, but the tendency of nucleic acid-dependent decrease of its activity was similar to the CXCR4 targeting polycation and peptide. In our case, nucleic acid-dependent decrease of Bim activity was alleviated using a photosensitizer and light. In addition to the photosensitizing strategy, this issue might be avoided completely by designing a CPP—Bim fusion peptide connected using a disulfide bond, which is cleaved in a reductive intracellular environment.

The photo-assisted apoptosis-induction strategy can be applied to *in vivo* cancer treatment using photosensitizers excitable by near-infrared light which can penetrate deep tissues (34). In addition, the tumor selectivity of the nanocomplex should be considered for future *in vivo* applications. In case of PEG-oligocholic acid-based micellar nanoparticles, cationic nanoparticles exhibit undesirable liver accumulation (35). Thus, the cationic nature of the complex may be disadvantageous for *in vivo* use. However, the CPP-based nanocomplex including siRNA clearly demonstrated antitumor activity with no *in vivo* toxicity, despite having a highly cationic surface charge (36). This report suggests that TatBim/miR-34a could offer *in vivo* effectiveness. Further, introduction of cancer-targeting moieties, such as the peptides F3 (37) and RGD (38), into the nanocomplex or substituting Tat with tumor-homing CPP (39) would increase tumor specificity of the nanocomplex.

In conclusion, we succeeded in the preparation of TatBim/RNA nanocomplexes with bean-like structures (diameters ranging from 215 to 330 nm) and efficient delivery of the complexes into cells. Our focus was on the combined biological effect of the peptide and RNA in the peptide/RNA complex. By using a photosensitizing strategy, the combined apoptotic effects of the peptide and RNA were successfully demonstrated. Our present study provided a guideline of designing light-dependent peptide and RNA dual delivery systems with effective releasing capacity in intracellular compartments.

Supplementary data to this article can be found online at https://doi.org/10.1016/j.jbiosc.2019.01.003.

ACKNOWLEDGMENTS

We thank Dr. K. Watanabe (Okayama University) for the preparation of the RNA, Dr. T. Uchida and Ms. M. Yoneda (Okayama University) for their support in the STEM and EDS analyses, and Prof. T. Ono (Okayama University) for his support in the Dynamic light scattering analyses. This work was supported by Okayama Foundation for Science and Technology.

References

1. **Chen, C., Li, L., Lodish, H. F., and Bartel, D. P.:** MicroRNAs modulate hematopoietic lineage differentiation, Science, **303**, 83—86 (2004).
2. **Chen, J.-F., Mandel, E. M., Thomson, J. M., Wu, Q., Callis, T. E., Hammond, S. M., Conlon, F. L., and Wang, D.-Z.:** The role of microRNA-1 and microRNA-133 in skeletal muscle proliferation and differentiation, Nat. Genet., **38**, 228—233 (2006).
3. **Carrington, J. C. and Ambros, V.:** Role of microRNAs in plant and animal development, Science, **301**, 336—338 (2003).
4. **Kloosterman, W. P., Lagendijk, A. K., Ketting, R. F., Moulton, J. D., and Plasterk, R. H. A.:** Targeted inhibition of miRNA maturation with morpholinos reveals a role for miR-375 in pancreatic islet development, PLoS Biol., **5**, 1738—1749 (2007).
5. **Jordan, S. D., Krüger, M., Willmes, D. M., Redemann, N., Wunderlich, F. T., Brönneke, H. S., Merkwirth, C., Kashkar, H., Olkkonen, V. M., Böttger, T., and other 3 authors:** Obesity-induced overexpression of miRNA-143 inhibits insulin-stimulated AKT activation and impairs glucose metabolism, Nat. Cell Biol., **13**, 434—446 (2011).
6. **Wilfred, B. R., Wang, W. X., and Nelson, P. T.:** Energizing miRNA research: a review of the role of miRNAs in lipid metabolism, with a prediction that miR-103/107 regulates human metabolic pathways, Mol. Genet. Metab., **91**, 209—217 (2007).
7. **Hwang, H. W. and Mendell, J. T.:** MicroRNAs in cell proliferation, cell death, and tumorigenesis, Br. J. Cancer, **94**, 776—780 (2007).
8. **Aagaard, L. and Rossi, J. J.:** RNAi therapeutics: principles, prospects and challenges, Adv. Drug Deliv. Rev., **59**, 75—86 (2007).
9. **Bader, A. G., Brown, D., and Winkler, M.:** The promise of microRNA replacement therapy, Cancer Res., **70**, 7027—7030 (2010).
10. **Hoyer, J. and Neundorf, I.:** Peptide vectors for the nonviral delivery of nucleic acids, Acc. Chem. Res., **45**, 1048—1056 (2012).
11. **Endoh, T. and Ohtsuki, T.:** Cellular siRNA delivery using cell-penetrating peptides modified for endosomal escape, Adv. Drug Deliv. Rev., **61**, 704—709 (2009).
12. **Copolovici, D. M., Langel, K., Eriste, E., and Langel, Ü.:** Cell-penetrating peptides: design, synthesis, and applications, ACS Nano, **8**, 1972—1994 (2014).
13. **Boisguerin, P., Deshayes, S., Gait, M. J., O'Donovan, L., Godfrey, C., Betts, C. A., Wood, M. J. A., and Lebleu, B.:** Delivery of therapeutic oligonucleotides with cell penetrating peptides, Adv. Drug Deliv. Rev., **87**, 52—67 (2015).
14. **De Fougerolles, A., Vornlocher, H.-P., Maraganore, J., and Lieberman, J.:** Interfering with disease: a progress report on siRNA-based therapeutics, Nat. Rev. Drug Discov., **6**, 443—453 (2007).
15. **Lundberg, P., El-Andaloussi, S., Sütlü, T., Johansson, H., and Langel, Ü.:** Delivery of short interfering RNA using endosomolytic cell-penetrating peptides, FASEB J., **21**, 2664—2671 (2007).
16. **Hou, K. K., Pan, H., Lanza, G. M., and Wickline, S. A.:** Melittin derived peptides for nanoparticle based siRNA transfection, Biomaterials, **34**, 3110—3119 (2013).

17. **Hou, K. K., Pan, H., Ratner, L., Schlesinger, P. H., and Wickline, S. A.:** Mechanisms of nanoparticle-mediated siRNA transfection by melittin-derived peptides, ACS Nano, **7**, 8605–8615 (2013).
18. **Xu, W., Pan, R., Zhao, D., Chu, D., Wu, Y., Wang, R., Chen, B., Ding, Y., Sadatmousavi, P., Yuan, Y., and Chen, P.:** Design and evaluation of endosomolytic biocompatible peptides as carrier for siRNA delivery, Mol. Pharm., **12**, 56–65 (2015).
19. **Wadia, J. S., Stan, R. V., and Dowdy, S. F.:** Transducible TAT-HA fusogenic peptide enhances escape of TAT-fusion proteins after lipid raft macropinocytosis, Nat. Med., **10**, 310–315 (2004).
20. **Kashiwagi, H., McDunn, J. E., Goedegebuure, P. S., Gaffney, M. C., Chang, K., Trinkaus, K., Piwnica-Worms, D., Hotchkiss, R. S., and Hawkins, W. G.:** TAT-Bim induces extensive apoptosis in cancer cells, Ann. Surg. Oncol., **14**, 1763–1771 (2007).
21. **Watanabe, K., Fujiwara, H., Kitamatsu, M., and Ohtsuki, T.:** Photoinduced apoptosis using a peptide carrying a photosensitizer, Bioorg. Med. Chem. Lett., **26**, 3115–3118 (2016).
22. **He, L., He, X., Lim, L. P., De Stanchina, E., Xuan, Z., Liang, Y., Xue, W., Zender, L., Magnus, J., Ridzon, D., and other 6 authors:** A microRNA component of the p53 tumour suppressor network, Nature, **447**, 1130–1134 (2007).
23. **Wiggins, J. F., Ruffino, L., Kelnar, K., Omotola, M., Patrawala, L., Brown, D., and Bader, A. G.:** Development of a lung cancer therapeutic based on the tumor suppressor microRNA-34, Cancer Res., **70**, 5923–5930 (2010).
24. **Kasinski, A. L. and Slack, F. J.:** MiRNA-34 prevents cancer initiation and progression in a therapeutically resistant K-ras and p53-induced mouse model of lung adenocarcinoma, Cancer Res., **72**, 5576–5587 (2012).
25. **Heitz, F., Morris, M. C., and Divita, G.:** Twenty years of cell-penetrating peptides: from molecular mechanisms to therapeutics, Br. J. Pharmacol., **157**, 195–206 (2009).
26. **Erazo-Oliveras, A., Najjar, K., Dayani, L., Wang, T.-Y., Johnson, G. A., and Pellois, J.-P.:** Protein delivery into live cells by incubation with an endosomolytic agent, Nat. Methods, **11**, 861–867 (2014).
27. **Järver, P., Mäger, I., and Langel, Ü.:** In vivo biodistribution and efficacy of peptide mediated delivery, Trends Pharmacol. Sci., **31**, 528–535 (2010).
28. **Endoh, T., Sisido, M., and Ohtsuki, T.:** Cellular siRNA delivery mediated by a cell-permeant RNA-binding protein and photoinduced RNA interference, Bioconjug. Chem., **19**, 1017–1024 (2008).
29. **Endoh, T., Sisido, M., and Ohtsuki, T.:** Spatial regulation of specific gene expression through photoactivation of RNAi, J. Control. Release, **137**, 241–245 (2009).
30. **Matsushita-Ishiodori, Y., Morinaga, M., Watanabe, K., and Ohtsuki, T.:** Near-infrared light-directed RNAi using a photosensitive carrier molecule, Bioconjug. Chem., **24**, 1669–1673 (2013).
31. **Ohtsuki, T., Miki, S., Kobayashi, S., Haraguchi, T., Nakata, E., Hirakawa, K., Sumita, K., Watanabe, K., and Okazaki, S.:** The molecular mechanism of photochemical internalization of cell penetrating peptide-cargo-photosensitizer conjugates, Sci. Rep., **5**, 18577 (2015).
32. **Li, J., Zhu, Y., Hazeldine, S. T., Li, C., and Oupický, D.:** Dual-function CXCR4 antagonist polyplexes to deliver gene therapy and inhibit cancer cell invasion, Angew. Chem. Int. Ed., **51**, 8740–8743 (2012).
33. **Egorova, A., Shubina, A., Sokolov, D., Selkov, S., Baranov, V., and Kiselev, A.:** CXCR4-targeted modular peptide carriers for efficient anti-VEGF siRNA delivery, Int. J. Pharm., **515**, 431–440 (2016).
34. **Plaetzer, K., Krammer, B., Berlanda, J., and Berr, F.:** Photophysics and photochemistry of photodynamic therapy : fundamental aspects, Lasers Med. Sci., **24**, 259–268 (2009).
35. **Xiao, K., Li, Y., Luo, J., Lee, J. S., Xiao, W., Gonik, A. M., Agarwal, R. G., and Lam, K. S.:** The effect of surface charge on in vivo biodistribution of PEG-oligocholic acid based micellar nanoparticles, Biomaterials, **32**, 3435–3446 (2011).
36. **Won, Y.-W., Yoon, S.-M., Lee, K.-M., and Kim, Y.-H.:** Poly(oligo-D-arginine) with internal disulfide linkages as a cytoplasm-sensitive carrier for siRNA delivery, Mol. Ther., **2**, 372–380 (2011).
37. **Reddy, G. R., Bhojani, M. S., Mcconville, P., Moody, J., Moffat, B. A., Hall, D. E., Kim, G., Koo, Y. L., Woolliscroft, M. J., Sugai, J. V., and other 5 authors:** Vascular targeted nanoparticles for imaging and treatment of brain tumors, Clin. Cancer Res., **12**, 6677–6687 (2006).
38. **Arap, W., Pasqualini, R., and Ruoslahti, E.:** Cancer treatment by targeted drug delivery to tumor vasculature in a mouse model, Science, **279**, 377–380 (1998).
39. **Kondo, E., Saito, K., Tashiro, Y., Kamide, K., Uno, S., Furuya, T., Mashita, M., Nakajima, K., Tsumuraya, T., Kobayashi, N., and other 3 authors:** Tumor lineage-homing cell-penetrating peptides as anticancer molecular delivery, Nat. Commun., **3**, 951 (2012).